Editors' Suggestion | Featured in Physics

Experimental Observation of Single- and Multisite Matter-Wave Solitons in an Optical Accordion Lattice

Robbie Cruickshank,[1] Francesco Lorenzi,[2,3] Arthur La Rooij,[1] Ethan F. Kerr,[1] Timon Hilker,[1] Stefan Kuhr,[1] Luca Salasnich,[2,4,3,5] and Elmar Haller[1]

[1]Department of Physics and SUPA, University of Strathclyde, Glasgow G4 0NG, United Kingdom
[2]Dipartimento di Fisica e Astronomia "Galileo Galilei," Università di Padova, Via Marzolo 8, 35131 Padova, Italy
[3]Istituto Nazionale di Fisica Nucleare, Sezione di Padova, Via Marzolo 8, 35131 Padova, Italy
[4]Padua QTech Center, Universita di Padova, Via Marzolo 8, 35131 Padova, Italy
[5]Istituto Nazionale di Ottica del Consiglio Nazionale della Ricerche, Unit of Sesto Fiorentino, Via Carrara 1, 50019 Sesto Fiorentino, Italy

(Received 15 April 2025; accepted 16 October 2025; published 23 December 2025)

We report the experimental observation of discrete bright matter-wave solitons with attractive interaction in an optical lattice. Using an accordion lattice with adjustable spacing, we prepare a Bose-Einstein condensate of cesium atoms across a defined number of lattice sites. By quenching the interaction strength and the trapping potential, we generate both single-site and multisite solitons. Our results reveal the existence and characteristics of these solitons across a range of lattice depths and spacings. We identify stable regions of the solitons based on interaction strength and lattice properties, and compare these findings with theoretical predictions. The experimental results qualitatively agree with a Gaussian variational model and match quantitatively with numerical simulations of the three-dimensional Gross-Pitaevskii equation extended with a quintic term to account for the loss of atoms. Our results provide insights into the quench dynamics and collapse mechanisms, paving the way for further studies of transport and dynamical properties of matter-wave solitons in lattices.

DOI: 10.1103/sh72-wnmv

Bright solitons are localized wave packets that propagate without spreading over a low-intensity background in a nonlinear medium [1]. They arise when the nonlinear self-focusing in the medium balances the dispersive spreading of the wave. Bright solitons have been observed in various physical systems, including optical fibers [2], fluids [3], and quantum gases [4]. In particular, Bose-Einstein condensates with attractive interactions have been instrumental in studying matter-wave solitons in homogeneous systems, experimentally demonstrating the formation [5–7], collapse [8–10], and collisions [11] of bright solitons.

Based on a seminal theoretical insight by Davydov and Kislukha [12], solitons have also been studied in systems with periodic potentials. Such "lattice solitons" [13] arise in wide range of systems [14], including molecular chains [12,15], nonlinear optical waveguide arrays [16–19], and quantum gases in optical lattices [20–22]. They exist in both one-dimensional and two-dimensional geometries [17,23–25] and are predicted to exhibit intricate transport properties [20,23,26,27]. However, despite considerable theoretical interest [20,28–35], the experimental realization of lattice solitons with attractive matter waves has remained an open challenge.

Lattice solitons can be classified into single-site (SS) and multisite (MS) solitons, which extend over different numbers of lattice sites, as well as on-site and off-site solitons, which are centered directly on sites or between them [31]. In this Letter, we provide an experimental demonstration of both single-site and multisite solitons of attractively interacting matter waves. These solitons form near the center of the Brillouin zone with energies below the lowest lattice band [29,36]. This is in contrast to gap solitons with repulsive interactions [22,37] that appear in the energy gap near the band edge. We investigate the solitons' stability and decay dynamics, and compare our findings with theoretical predictions. A key element of our experimental approach is an accordion lattice with variable lattice spacing d_L [38–40], which serves three primary roles: the preparation of an initial wave packet in a given number of sites, the study of solitons for varying lattice spacing, and a magnification scheme for an improved detection of the soliton's density distribution.

In addition to studying the soliton's density profile along the lattice direction, we found it important to also include its radial profile and three-body loss in our models.

Although not limiting, three-body loss is non-negligible due to the increased density arising from lattice confinement and attractive interactions. To capture the soliton's full dynamical behavior, we numerically solved the three-dimensional Gross-Pitaevskii equation (3D GPE) with an added quintic loss term [41–43]. However, we start by analyzing the system with a variational approach based on a Gaussian ansatz [31] to provide initial insight into the soliton's stability and the underlying physical mechanisms.

Within this model, the energy of a Gaussian wave packet with axial length η and radial width σ is given by

$$E = \frac{1}{2}\left(\frac{1}{2\eta^2} + \frac{1}{\sigma^2} + \sigma^2\right) + \frac{g}{2\sqrt{2\pi}\sigma^2\eta} - V_0 \exp(-k_L^2\eta^2). \quad (1)$$

Here, η, σ are in units of the radial harmonic oscillator length $a_\perp = \sqrt{\hbar/m\omega_\perp}$, and E is in units of $\hbar\omega_\perp$, where $\omega_\perp$ is the radial trap frequency and m is the atomic mass. The first term in Eq. (1) provides the kinetic energy of the soliton, while the second term describes the interaction energy using the interaction strength $g = 2a_s N/a_\perp$, where a_s is the s-wave scattering length and N the total atom number. The third term contains the lattice contribution, with lattice depth V_0 in units of $\hbar\omega_\perp$ and wave number $k_L = \pi/d_L$. For a simplified illustration [Fig. 1(a)], we

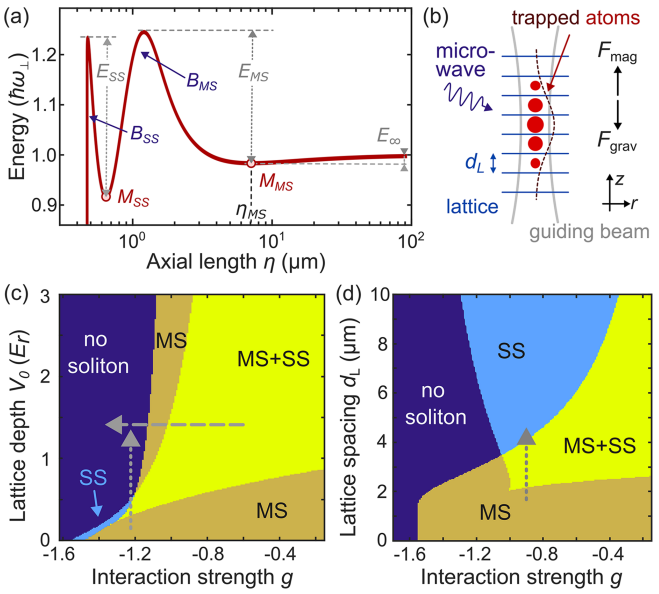

FIG. 1. Experimental setup and stability diagrams. (a) Energy $E(\eta)$ for a Gaussian wave packet with $V_0 = 1.1E_r$, $a_s = -6.2a_0$, $d_L = 2$ μm. SS and MS solitons are stable at minima M_{SS} and M_{MS} with barriers B_{SS} and B_{MS}. (b) Sketch of the experimental setup. (c) Stable regions of SS and MS solitons for varying parameters g and V_0, with $N = 1800$, $\omega_\perp = 2\pi \times 30$ Hz, $d_L = 3.2$ μm. No solitons exist in dark blue regions. (d) Stable regions for varying d_L; same parameters as (c) with constant $V_0 = 1.3E_r$ set at $d_L = 3.2$ μm.

determined the value σ_{min} that minimizes $E(\eta, \sigma)$ for each value of η [44,45]. The resulting energy $E(\eta) = E(\eta, \sigma_{min}(\eta))$ shows two minima where stable single-site and multisite solitons form [M_{SS} and M_{MS} in Fig. 1(a)]. Collapse toward smaller axial length η is prevented by two barriers B_{SS} and B_{MS}.

Without a lattice potential, there is only one barrier with a single critical interaction strength g_c [45], beyond which the barrier disappears and the wave packet collapses. The value of g_c depends on geometry and confinement, and various methods have been used for its predictions, e.g., numerically solving the full 3D Gross-Pitaevskii equation [44,46] with a variational approach [44,47], or using the nonpolynomial Gross-Pitaevskii equation [48]. With a lattice potential, the barrier heights depend also on lattice depth and spacing, and g_c is replaced by surfaces in the (g, V_0, d_L)-parameter space that indicate the disappearance of the barriers.

The patches in Figs. 1(c) and 1(d) represent stable regions with nonzero energy barriers for parameters (g, V_0) and (g, d_L). The critical interaction strength is given by the boundary that separates parameter regions without solitons (dark blue patches) and with solitons ("SS" and "MS"). The interplay between V_0, d_L, and g and the barrier heights E_{SS} and E_{MS} is not straightforward. For instance, decreasing g at a fixed lattice depth [dashed horizontal arrow in Fig. 1(c)] lowers the barriers due to strong attractive interactions and leads to the eventual collapse, first of the single-site soliton followed by the multisite soliton. Conversely, when the interaction strength is held constant [dotted vertical arrow in Fig. 1(c)], the multisite soliton can already exist at shallow lattice depths, whereas a larger value of V_0 is required to form the energy minimum M_{SS} that supports the single-site soliton. A further increase of V_0 eventually eliminates both barriers. Both types of solitons connect to bright 1D solitons without a lattice, either in the limit of vanishing lattice depth or in the limit of large lattice spacing for single-site solitons [49].

In our experiment, we created a magnetically levitated Bose-Einstein condensate of $N \approx 1.3 \times 10^5$ cesium atoms in a crossed-beam dipole trap at a wavelength of 1064 nm [52,53]. A broad magnetic Feshbach resonance in the $F = 3, m_F = 3$ state with a zero crossing at 17.1 G allowed us to tune interactions [54,55]. To reduce the atom number, we lowered the levitation gradient over three seconds ($N \approx 30000$ atoms) before transferring the condensate into our accordion lattice at 780 nm. All but a few central sites were then selectively cleared using a combination of microwave transfer and resonant light ($N \lesssim 3000$ atoms) [Fig. 1(b)] [56]. During the transfer, we set $d_L = 3.2(2)$ μm and $V_0 \approx 100E_r$ to simplify the spatial site selection in the levitation gradient. V_0 is always given in recoil energy $E_r = (\hbar\pi/d_L)^2/(2m)$, where d_L is the lattice spacing specific to each measurement. While we can remove 95% of the atoms per site without affecting neighbors,

here we increased the removal to close to 100% at the cost of 5% loss in neighboring sites (for further details, see Refs. [49,57]).

To prepare the initial density profile of the wave packet before the interaction quench, we added a dipole trap with frequency ω_z [dashed line Fig. 1(b)], adjusted both d_L and V_0 to their final values, and tuned a_s to approximately $+20a_0$ in 400 ms, where a_0 is Bohr's radius. An additional waiting period of 200 ms ensured phase coherence between the sites, which we verified through free expansion measurements. Finally, we created the solitons by quenching a_s to negative values and by removing the longitudinal trapping potential within 2 ms. After an evolution time t, we used a magnification scheme to analyze the density distribution of the wave packet with absorption imaging [39]. The lattice depth V_0 was increased to approximately $100E_r$, effectively freezing the atom distribution within the sites, followed by a slow expansion of d_L to 20(1) μm over a period of 400 ms.

In the first measurement, we demonstrated the existence and properties of single-site solitons. After preparing approximately 1800 atoms at a single site, we quenched a_s and measured the density profile and the atom number per lattice site after a hold time of 100 ms. Absorption images of the density profile show a strong dependence on a_s [Fig. 2(a)]. For $a_s \approx -8a_0$, the wave packet remained localized at the central lattice site, which indicated the formation of a single-site soliton. Except for some initial shedding of atoms, we found this soliton to be stable for a hold time up to 2 s [49]. For stronger attractive interaction, $a_s < -10a_0$, the soliton collapsed, and the remaining atoms spread along the lattice direction. Weak attractive and repulsive interactions $-5a_0 < a_s < +5a_0$ resulted in the dispersion of the wave packet, with a minimum at the central lattice site after the given hold time, while larger scattering lengths $a_s > +7a_0$ led again to the localization of the wave packet. In the two-particle limit, this localized state corresponds to repulsively bound pairs [58], whereas in the context of two lattice sites and Josephson oscillations, it is associated with macroscopic quantum self-trapping [59,60].

We extended the study to different lattice depths and determined the relative atom number in the central site N_c/N as a measure of the system stability [Fig. 2(b)]. The data reveal the three regimes: (i) a stable single-site soliton, (ii) a free dispersion of the wave packet close to $0a_0$, and (iii) the self-trapping for repulsive interaction and sufficient lattice depth. The regimes can be explained by the height of the barriers B_{SS} and B_{MS}. For comparison, Fig. 2(c) shows the energy E_{SS}, which is the height of barrier B_{SS} [see Fig. 1(a) and [49]]. Large values of E_{SS} align well with the experimental data in Fig. 2(c), accurately predicting the stable regions (i) and (iii). However, E_{SS} does not capture the evolution of the wave packet close to zero scattering length in region (ii), where the wave packet spreads. While

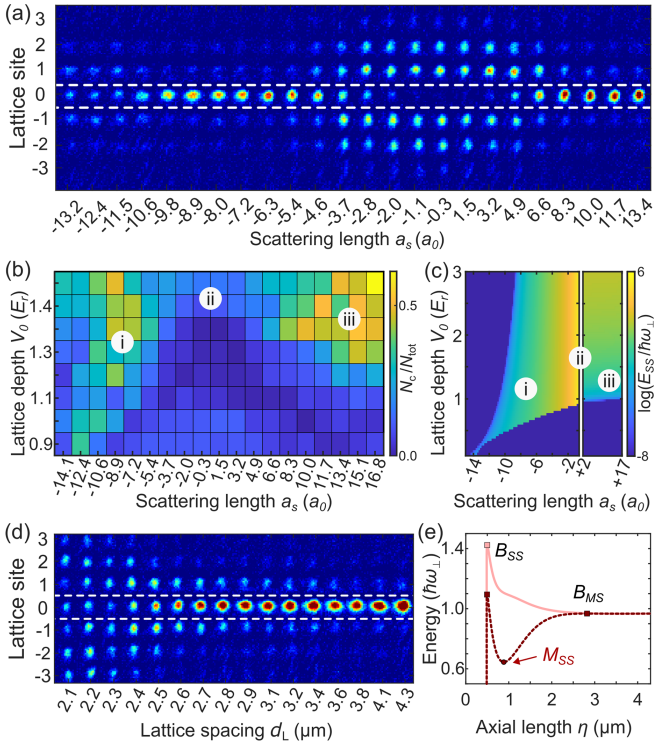

FIG. 2. Stability of single-site solitons. (a) Measured density distribution after a quench of a_s and $t = 100$ ms hold time with $d_L = 3.2(2)$ μm, $V_0 = 1.3(1)E_r$, $\omega_\perp = 2\pi \times 40(1)$ Hz, $N \approx 1800$. White lines mark atoms in the central site. (b) Measured relative central-site atom number N_c/N_{tot} vs a_s and V_0 with the same parameters as (a). (c) Energy E_{SS} of the barrier B_{SS}; (i)–(iii) indicate regions of varying stability in (b),(c). See Ref. [49] for the definition of E_{SS} for $a_s > 0a_0$. (d) Density distribution for varying d_L after 100 ms with $a = -6.4a_0$, $N \approx 1800$, constant $V_0 = 1.3(1)E_r$ set at $d_L = 3.2(2)$ μm. (e) Calculated $E(\eta)$ for (d) with $d_L = 3.5$ μm (dotted line) and $d_L = 2.0$ μm (solid line). Measured data are averaged over typically seven repetitions.

collapse is prevented by barrier B_{SS}, spreading is inhibited by the barriers at larger values of η [Fig. 1(a)].

To investigate the effect of the lattice spacing on the stability of the solitons, we varied d_L while keeping V_0 and a_s constant [Fig. 2(d)]. Absorption images taken after a hold time of 100 ms show a spreading of the wave packet for $d_L \lesssim 2.5$ μm [Fig. 2(d)]. Our calculations of $E(\eta)$ indicate that as d_L decreases, the minimum M_{SS} disappears, while the barrier B_{SS} persists [Fig. 2(e)]. Consequently, the observed spreading after the interaction quench is not due to a collapse, as observed in Fig. 2(a), but rather due to the absence of an energy minimum. The calculated minimum M_{SS} vanishes for $d_L \approx 2.2$ μm, which agrees with our experimental data ($d_L \approx 2.5$ μm). This measurement also aligns well with the stability diagram in Fig. 1(d) (dotted arrow).

In the second measurement, we investigated the stability of multisite wave packets. To prepare the initial state, we

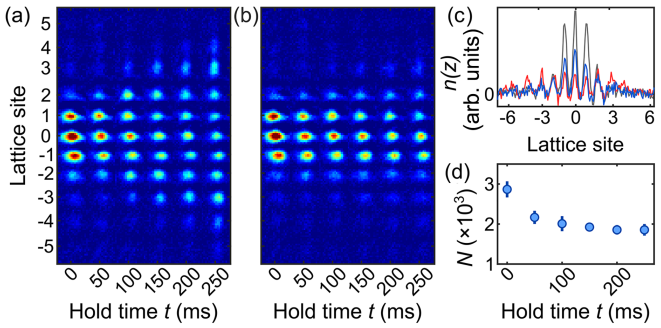

FIG. 3. Stability of a multisite wave packet. (a),(b) Time evolution of a wave packet after a quench of a_s averaged over ten repetitions with $V_0 = 1.3E_r$, $d_L = 2.6$ μm, $\omega_\perp = 2\pi \times 25$ Hz, $\omega_z = 2\pi \times 25$ Hz, $N \approx 2900$. (a) The wave packet disperses for a quench to $a_s = +2.0a_0$ and (b) mostly retains its overall shape for $-5.7a_0$. Site occupation numbers for both datasets are provided in Ref. [49]. (c) Density profiles of the wave packet immediately after the quench (gray), and after 250 ms for $+2.0a_0$ (red) and $-5.7a_0$ (blue). (d) Atom number for data in (b); error bars denote the standard deviation. A comparison of the data in (c),(d) with a 3D-GPE simulation is provided in Ref. [49].

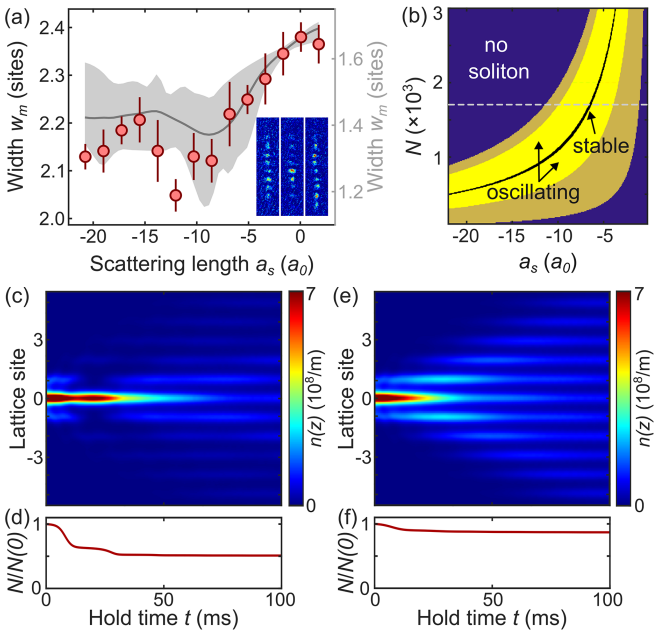

FIG. 4. Collapse of a multisite wave packet. (a) Width w_m of the wave packet at $t = 150$ ms after quenching to different values of a_s, with $V_0 = 1.4E_r$, $d_L = 2.6$ μm, $\omega_\perp = 2\pi \times 30$ Hz, $N \approx 1700$. The gray patch shows the variation in w_m calculated using the 3D GPE, resulting from uncertainties in the three-body loss coefficient L_3 and N. The line is an average of the calculations [49]. Inset, left to right: typical images of the density profiles after collapse ($a_s = -17a_0$) shrinking toward the central site ($a_s = -10a_0$) and expanding wave packet ($a_s = 0a_0$). (b) Stability regions calculated using Eq. (1) with an existing minimum M_{MS} (brown) and without (blue), with breathing oscillations for $E(\eta) < E_\infty$ and E_{MS} (yellow), and with stable multisite solitons for $E(\eta_0) \approx E_{MS}$ (black). (c),(d) The calculated time evolution of the density distribution and relative atom number show collapse followed by expansion for $a_s = -9.5a_0$, and (e),(f) dispersion for $a_s = -1.7a_0$. Calculations use $L_3 = 5 \times 10^{-39}$ m^6 s^{-1} and other parameters as in (a).

adjusted the microwave transfer to remove all but the atoms in three adjacent lattice sites. During the subsequent waiting period, this density profile evolved toward a Gaussian envelope spanning three to five lattice sites determined by the trapping frequency ω_z. After the quench, we observed stronger density fluctuations compared to single-site solitons, showing in some cases a splitting of the soliton with moving fractions. Quantum fluctuations have been suggested as a possible cause of this fragmentation [61–63]. However, here, we attributed it to technical noise and the low binding energy of multisite solitons E_∞ [Fig. 1(a)].

We studied the time evolution of the wave packet over 250 ms following the quench. For scattering lengths near zero [Fig. 3(a)], the wave packet shows dispersion, whereas for $a_s = -5.7a_0$ [Fig. 3(b)], it remains mostly localized. We attribute this localization to the formation of a multisite solitonlike state. The density profiles show little change in site occupations between $t = 100$ and 250 ms, indicating a stable configuration. However, during the initial tens of milliseconds, we observe a loss of atoms in the three central sites. We attribute this initial depletion to three-body loss, which predominantly occurs in high-density regions where attractive interactions enhance the local density [64]. The subsequent atom loss is strongly reduced, and we speculate that the wave packet gradually adjusts its radial and axial sizes in response to the slowly decreasing atom number.

The 1D density profiles [Fig. 3(c)] and the measured total atom number [Fig. 3(d)] support this interpretation. Comparing the initial 1D density profile [gray line in Fig. 3(c)] with the profile after 250 ms reveals a reduction in atom number at the three central sites for the solitonlike wave packet (blue line), while the overall profile remains localized. In contrast, for near-zero interactions (red line), the wave packet undergoes significant spreading, with increased occupation of the outermost sites. To quantify the spreading, we calculated the relative site occupations N_j/N and extracted the wave packet width [49]. The noninteracting and solitonlike wave packets exhibit linear dispersion velocities of 12 and 7 sites/s, respectively. For the solitonlike wave packet, this apparent spreading mainly reflects the flattening of the density profile rather than significant mass transport. We also found good agreement of the density profiles and atom numbers in Figs. 3(c) and 3(d) with simulations of the 3D GPE [49].

Finally, we quantitatively analyzed the collapse by measuring the wave packets' density profiles at $t = 150$ ms over a broad range of scattering lengths [Fig. 4(a)]. To account for varying density distributions, we calculated the second-moment width w_m of the site occupations defined as

$$w_m^2 = \frac{1}{N}\sum_j N_j (z_j - \bar{z})^2, \quad \text{with} \quad j = -4, \ldots, 4.$$

Here, z_j is the position of the jth lattice site, and $\bar{z}$ is the center-of-mass position. The value of w_m indicates the varying stability of the wave packet depending on a_s. It spreads for $a_s \approx 0a_0$, shrinks toward the central site for $a_s \approx -10a_0$, and spreads after collapse for strong attractive interactions $a_s < -13a_0$. Single absorption images illustrate the spreading and shrinking of the wave packet in the different regions [inset in Fig. 4(a)].

The variational approach used in Eq. (1) provides a simple model for predicting the evolution of the wave packet after quenching to scattering length a_s. Within the model, stability is achieved when the initial parameters of the wave packet $N(0)$ and η_0 closely match those of a multisite soliton with length η_{MS}. In our experimental protocol, $N(0)$ and η_0 are set during preparation, while only a_s can be varied. A soliton is created by quenching the scattering length to a_s^* with $\eta_0 = \eta_{\mathrm{MS}}(N(0), a_s^*)$. For other quench values close to a_s^*, the wave packet is expected to exhibit small breathing oscillations [31], unless its initial energy $E(\eta_0)$ exceeds one of the barrier energies E_∞ or E_{MS}, leading to dispersion or collapse. Calculating the barrier energy barriers E_∞ and E_{MS} using Eq. (1) allows us to predict the stability regions. The brown patch in Fig. 4(b) marks where a minimum M_{MS} exists. Stable solitons form only along the black line, while breathing oscillations occur within the yellow regions. Assuming a fixed atom number further constrains the choice of a_s to lie on the dashed line, though in practice N decreases due to three-body loss.

To capture the full evolution of the wave packet beyond this simple model, we numerically simulated the dynamics of the multisite soliton using a modified GPE with a quintic term that accounts for three-body loss [41,42,49]. The simulations show two distinct dynamical regimes. In the first regime, corresponding to large negative values of a_s, the wave packet begins to collapse, leading to an increase in local density at the central site [Fig. 4(c)]. However, a further shrinking of the wave packet is suppressed by the enhanced loss and a rapid shedding of atoms [Fig. 4(d)]. The second regime, which occurs for less negative values of a_s, is marked by a slow dispersion of the matter wave, and has lower and more gradual atom loss [Figs. 4(e) and 4(f)].

The simulation agrees well with the observed shrinking in w_m during the collapse process. However, it is sensitive to the precise values of atom number and the three-body loss coefficient [64,65], resulting in an uncertainty of the predicted dynamics [gray patch in Fig. 4(a)] [49]. In addition, imaging noise in the experimental data increases w_m, leading to an offset and reduced contrast compared to the simulation. While the observed atom loss was sufficiently low to permit the formation and investigation of lattice solitons, its inclusion in our simulation was still essential to reproduce our observations. Interestingly, at strong attractive interactions, the loss helped to suppress collapse and enhanced the stability of the system.

In conclusion, we have demonstrated the existence and stability of both single-site and multisite solitons that extend over varying numbers of lattice sites. Using an accordion lattice with adjustable lattice spacing, we examined their properties across various lattice depths and spacings, and compared our findings with theoretical predictions. A variational model based on a Gaussian approximation for the solitons was used to identify stable parameter regions, while numerical simulations of the 3D GPE with a three-body loss term captured the solitons' time evolution. We found both types of solitons to be stable for hundreds of milliseconds, allowing ample time for further studies.

Our results pave the way for exploring a multitude of nonlinear matter-wave excitations in optical lattices, such as lattice breathers [66] and discrete solitons in deep lattice potentials, described by the discrete nonlinear Schrödinger equation [32,67]. For example, our approach allows us to investigate the Peierls-Nabarro barrier [23], probe 2D solitons [24], and experimentally access the dynamical phase diagram [20,27], which predicts the emergence of breathers and solitons as a function of the quasimomentum. Our results advance the understanding of nonlinear wave dynamics in structured media and open new avenues for technological applications, e.g., in matter-wave interferometry [68–70], precision sensing [71], and the controlled transport of atomic wave packets for quantum information processing [72,73].

Acknowledgments—We acknowledge support by the EPSRC through a New Investigator Grant (Grant No. EP/T027789/1), the Programme Grant "Quantum Advantage in Quantitative Quantum Simulation" (Grant No. EP/Y01510X/1), and the Quantum Technology Hub in Quantum Computing and Simulation (Grant No. EP/T001062/1). T. H. acknowledges funding from the European Research Council (ERC Starting Grant "FOrbQ" No. 101165353). F. L. and L. S. are supported by the "Iniziativa Specifica Quantum" of INFN and by the project "Frontiere Quantistiche" (Dipartimenti di Eccellenza) of the Italian Ministry of University and Research (MUR). L. S. is supported by the European Union through the European Quantum Flagship Project "PASQuanS2," the National Center for HPC, and the Big Data and Quantum Computing [Spoke 10: Quantum Computing]. L. S. also acknowledges funding by the PRIN project "Quantum Atomic Mixtures: Droplets, Topological Structures, and Vortices" of MUR.

Data availability—The data that support the findings of this article are openly available [74], embargo periods may apply.

[1] Y. S. Kivshar and B. A. Malomed, Dynamics of solitons in nearly integrable systems, Rev. Mod. Phys. **61**, 763 (1989).
[2] L. F. Mollenauer, R. H. Stolen, and J. P. Gordon, Experimental observation of picosecond pulse narrowing and solitons in optical fibers, Phys. Rev. Lett. **45**, 1095 (1980).

[3] Solitary Waves in Fluids, edited by R. Grimshaw, *Advances in Fluid Mechanics* (WIT Press, Southampton, 2007).

[4] F. Kh. Abdullaev, A. Gammal, A. M. Kamchatnov, and L. Tomio, Dynamics of bright matter wave solitons in a Bose–Einstein condensate, Int. J. Mod. Phys. B **19**, 3415 (2005).

[5] C. C. Bradley, C. A. Sackett, and R. G. Hulet, Bose-Einstein condensation of lithium: Observation of limited condensate number, Phys. Rev. Lett. **78**, 985 (1997).

[6] K. E. Strecker, G. B. Partridge, A. G. Truscott, and R. G. Hulet, Formation and propagation of matter-wave soliton trains, Nature (London) **417**, 150 (2002).

[7] L. Khaykovich, F. Schreck, G. Ferrari, T. Bourdel, J. Cubizolles, L. D. Carr, Y. Castin, and C. Salomon, Formation of a matter-wave bright soliton, Science **296**, 1290 (2002).

[8] C. A. Sackett, H. T. C. Stoof, and R. G. Hulet, Growth and collapse of a Bose-Einstein condensate with attractive interactions, Phys. Rev. Lett. **80**, 2031 (1998).

[9] J. M. Gerton, D. Strekalov, I. Prodan, and R. G. Hulet, Direct observation of growth and collapse of a Bose-Einstein condensate with attractive interactions, Nature (London) **408**, 692 (2000).

[10] E. A. Donley, N. R. Claussen, S. L. Cornish, J. L. Roberts, E. A. Cornell, and C. E. Wieman, Dynamics of collapsing and exploding Bose-Einstein condensates, Nature (London) **412**, 295 (2001).

[11] J. H. V. Nguyen, P. Dyke, D. Luo, B. A. Malomed, and R. G. Hulet, Collisions of matter-wave solitons, Nat. Phys. **10**, 918 (2014).

[12] A. S. Davydov and N. I. Kislukha, Solitary excitons in one-dimensional molecular chains, Phys. Status Solidi (b) **59**, 465 (1973).

[13] We follow the convention of using the term "soliton" instead of "solitary wave" for our nonintegrable system, as suggested by B. A. Malomed, *Soliton Management in Periodic Systems* (Springer, New York, 2006), p. 19.

[14] B. A. Malomed, *Soliton Management in Periodic Systems* (Springer Science, New York, 2006).

[15] N. I. Kruglov, Solitons in quasi-one-dimensional molecular chains, J. Phys. C **17**, L453 (1984).

[16] H. S. Eisenberg, Y. Silberberg, R. Morandotti, A. R. Boyd, and J. S. Aitchison, Discrete spatial optical solitons in waveguide arrays, Phys. Rev. Lett. **81**, 3383 (1998).

[17] R. Morandotti, U. Peschel, J. S. Aitchison, H. S. Eisenberg, and Y. Silberberg, Dynamics of discrete solitons in optical waveguide arrays, Phys. Rev. Lett. **83**, 2726 (1999).

[18] J. W. Fleischer, T. Carmon, M. Segev, N. K. Efremidis, and D. N. Christodoulides, Observation of discrete solitons in optically induced real time waveguide arrays, Phys. Rev. Lett. **90**, 023902 (2003).

[19] B. A. Malomed and D. Mihalache, Nonlinear waves in optical and matter-wave media: A topical survey of recent theoretical and experimental results, Rom. J. Phys. **64**, 106 (2019).

[20] A. Trombettoni and A. Smerzi, Discrete solitons and breathers with dilute Bose-Einstein condensates, Phys. Rev. Lett. **86**, 2353 (2001).

[21] E. A. Ostrovskaya and Y. S. Kivshar, Matter-wave gap solitons in atomic band-gap structures, Phys. Rev. Lett. **90**, 160407 (2003).

[22] B. Eiermann, Th. Anker, M. Albiez, M. Taglieber, P. Treutlein, K.-P. Marzlin, and M. K. Oberthaler, Bright Bose-Einstein gap solitons of atoms with repulsive interaction, Phys. Rev. Lett. **92**, 230401 (2004).

[23] V. Ahufinger, A. Sanpera, P. Pedri, L. Santos, and M. Lewenstein, Creation and mobility of discrete solitons in Bose-Einstein condensates, Phys. Rev. A **69**, 053604 (2004).

[24] B. B. Baizakov, B. A. Malomed, and M. Salerno, Multidimensional solitons in periodic potentials, Europhys. Lett. **63**, 642 (2003).

[25] J. W. Fleischer, M. Segev, N. K. Efremidis, and D. N. Christodoulides, Observation of two-dimensional discrete solitons in optically induced nonlinear photonic lattices, Nature (London) **422**, 147 (2003).

[26] V. A. Brazhnyi and B. A. Malomed, Dragging two-dimensional discrete solitons by moving linear defects, Phys. Rev. E **84**, 016608 (2011).

[27] R. Franzosi, R. Livi, G.-L. Oppo, and A. Politi, Discrete breathers in Bose-Einstein condensates, Nonlinearity **24**, R89 (2011).

[28] F. Kh. Abdullaev, B. B. Baizakov, S. A. Darmanyan, V. V. Konotop, and M. Salerno, Nonlinear excitations in arrays of Bose-Einstein condensates, Phys. Rev. A **64**, 043606 (2001).

[29] N. K. Efremidis and D. N. Christodoulides, Lattice solitons in Bose-Einstein condensates, Phys. Rev. A **67**, 063608 (2003).

[30] H. Sakaguchi and B. A. Malomed, Matter-wave solitons in nonlinear optical lattices, Phys. Rev. E **72**, 046610 (2005).

[31] L. Salasnich, A. Cetoli, B. A. Malomed, and F. Toigo, Nearly-one-dimensional self-attractive Bose-Einstein condensates in optical lattices, Phys. Rev. A **75**, 033622 (2007).

[32] A. Maluckov, L. Hadžievski, B. A. Malomed, and L. Salasnich, Solitons in the discrete nonpolynomial Schrödinger equation, Phys. Rev. A **78**, 013616 (2008).

[33] Y. V. Kartashov, B. A. Malomed, and L. Torner, Solitons in nonlinear lattices, Rev. Mod. Phys. **83**, 247 (2011).

[34] C. P. Rubbo, I. I. Satija, W. P. Reinhardt, R. Balakrishnan, A. M. Rey, and S. R. Manmana, Quantum dynamics of solitons in strongly interacting systems on optical lattices, Phys. Rev. A **85**, 053617 (2012).

[35] P. Naldesi, J. P. Gomez, B. Malomed, M. Olshanii, A. Minguzzi, and L. Amico, Rise and fall of a bright soliton in an optical lattice, Phys. Rev. Lett. **122**, 053001 (2019).

[36] P. J. Y. Louis, E. A. Ostrovskaya, C. M. Savage, and Y. S. Kivshar, Bose-Einstein condensates in optical lattices: Band-gap structure and solitons, Phys. Rev. A **67**, 013602 (2003).

[37] M. Mitchell, A. Di Carli, G. Sinuco-León, A. La Rooij, S. Kuhr, and E. Haller, Floquet solitons and dynamics of periodically driven matter waves with negative effective mass, Phys. Rev. Lett. **127**, 243603 (2021).

[38] L. Fallani, C. Fort, J. E. Lye, and M. Inguscio, Bose-Einstein condensate in an optical lattice with tunable spacing: Transport and static properties, Opt. Express **13**, 4303 (2005).

[39] S. Al-Assam, R. A. Williams, and C. J. Foot, Ultracold atoms in an optical lattice with dynamically variable periodicity, Phys. Rev. A **82**, 021604 (2010).

[40] J. L. Ville, T. Bienaimé, R. Saint-Jalm, L. Corman, M. Aidelsburger, L. Chomaz, K. Kleinlein, D. Perconte, S. Nascimbène, J. Dalibard, and J. Beugnon, Loading and compression of a single two-dimensional Bose gas in an optical accordion, Phys. Rev. A **95**, 013632 (2017).
[41] H. Saito and M. Ueda, Mean-field analysis of collapsing and exploding Bose-Einstein condensates, Phys. Rev. A **65**, 033624 (2002).
[42] S. K. Adhikari, Mean-field description of collapsing and exploding Bose-Einstein condensates, Phys. Rev. A **66**, 013611 (2002).
[43] Y. Kagan, A. Muryshev, and G. Shlyapnikov, Collapse and Bose-Einstein condensation in a trapped Bose gas with negative scattering length, Phys. Rev. Lett. **81**, 933 (1998).
[44] L. D. Carr and Y. Castin, Dynamics of a matter-wave bright soliton in an expulsive potential, Phys. Rev. A **66**, 063602 (2002).
[45] N. G. Parker, S. L. Cornish, C. S. Adams, and A. M. Martin, Bright solitary waves and trapped solutions in Bose-Einstein condensates with attractive interactions, J. Phys. B **40**, 3127 (2007).
[46] P. A. Ruprecht, M. J. Holland, K. Burnett, and M. Edwards, Time-dependent solution of the nonlinear Schrödinger equation for Bose-condensed trapped neutral atoms, Phys. Rev. A **51**, 4704 (1995).
[47] V. M. Pérez-García, H. Michinel, J. I. Cirac, M. Lewenstein, and P. Zoller, Dynamics of Bose-Einstein condensates: Variational solutions of the Gross-Pitaevskii equations, Phys. Rev. A **56**, 1424 (1997).
[48] L. Salasnich, A. Parola, and L. Reatto, Effective wave equations for the dynamics of cigar-shaped and disk-shaped Bose condensates, Phys. Rev. A **65**, 043614 (2002).
[49] See Supplemental Material at http://link.aps.org/supplemental/10.1103/sh72-wnmv for additional information, which includes Refs. [50,51].
[50] R. A. Williams, J. D. Pillet, S. Al-Assam, B. Fletcher, M. Shotter, and C. J. Foot, Dynamic optical lattices: Two-dimensional rotating and accordion lattices for ultracold atoms, Opt. Express **16**, 16977 (2008).
[51] T. C. Li, H. Kelkar, D. Medellin, and M. G. Raizen, Real-time control of the periodicity of a standing wave: An optical accordion, Opt. Express **16**, 5465 (2008).
[52] T. Kraemer, J. Herbig, M. Mark, T. Weber, C. Chin, H.-C. Nägerl, and R. Grimm, Optimized production of a cesium Bose-Einstein condensate, Appl. Phys. B **79**, 1013 (2004).
[53] A. Di Carli, C. D. Colquhoun, S. Kuhr, and E. Haller, Interferometric measurement of micro-g acceleration with levitated atoms, New J. Phys. **21**, 053028 (2019).
[54] M. Gustavsson, E. Haller, M. J. Mark, J. G. Danzl, G. Rojas-Kopeinig, and H.-C. Nägerl, Control of interaction-induced dephasing of bloch oscillations, Phys. Rev. Lett. **100**, 080404 (2008).
[55] M. Berninger, A. Zenesini, B. Huang, W. Harm, H.-C. Nägerl, F. Ferlaino, R. Grimm, P. S. Julienne, and J. M. Hutson, Feshbach resonances, weakly bound molecular states, and coupled-channel potentials for cesium at high magnetic fields, Phys. Rev. A **87**, 032517 (2013).
[56] B. Peaudecerf, M. Andia, M. Brown, E. Haller, and S. Kuhr, Microwave preparation of two-dimensional fermionic spin mixtures, New J. Phys. **21**, 013020 (2019).
[57] R. Cruickshank, A. L. Rooij, E. Kerr, T. Hilker, S. Kuhr, and E. Haller, Tunable optical lattices for the creation of matter-wave lattice solitons, arXiv:2509.22471.
[58] K. Winkler, G. Thalhammer, F. Lang, R. Grimm, J. Hecker Denschlag, A. J. Daley, A. Kantian, H. P. Büchler, and P. Zoller, Repulsively bound atom pairs in an optical lattice, Nature (London) **441**, 853 (2006).
[59] A. Smerzi, S. Fantoni, S. Giovanazzi, and S. R. Shenoy, Quantum coherent atomic tunneling between two trapped Bose-Einstein condensates, Phys. Rev. Lett. **79**, 4950 (1997).
[60] M. Albiez, R. Gati, J. Fölling, S. Hunsmann, M. Cristiani, and M. K. Oberthaler, Direct observation of tunneling and nonlinear self-trapping in a single bosonic Josephson junction, Phys. Rev. Lett. **95**, 010402 (2005).
[61] B. J. Dabrowska-Wüster, S. Wüster, and M. J. Davis, Dynamical formation and interaction of bright solitary waves and solitons in the collapse of Bose-Einstein condensates with attractive interactions, New J. Phys. **11**, 053017 (2009).
[62] A. I. Streltsov, O. E. Alon, and L. S. Cederbaum, Swift loss of coherence of soliton trains in attractive Bose-Einstein condensates, Phys. Rev. Lett. **106**, 240401 (2011).
[63] A. D. Martin and J. Ruostekoski, Quantum dynamics of atomic bright solitons under splitting and recollision, and implications for interferometry, New J. Phys. **14**, 043040 (2012).
[64] T. Weber, J. Herbig, M. Mark, H.-C. Nägerl, and R. Grimm, Three-body recombination at large scattering lengths in an ultracold atomic gas, Phys. Rev. Lett. **91**, 123201 (2003).
[65] P.-T. Kraemer, Few-body interactions in an ultracold gas of cesium atoms, Ph.D. thesis, Leopold-Franzens-Universität Innsbruck, 2006.
[66] S. Flach and A. V. Gorbach, Discrete breathers—advances in theory and applications, Phys. Rep. **467**, 1 (2008).
[67] G. Gligorić, A. Maluckov, L. Salasnich, B. A. Malomed, and Lj. Hadžievski, Two routes to the one-dimensional discrete nonpolynomial Schrödinger equation, Chaos **19**, 043105 (2009).
[68] G. D. McDonald, C. C. N. Kuhn, K. S. Hardman, S. Bennetts, P. J. Everitt, P. A. Altin, J. E. Debs, J. D. Close, and N. P. Robins, Bright solitonic matter-wave interferometer, Phys. Rev. Lett. **113**, 013002 (2014).
[69] J. L. Helm, S. L. Cornish, and S. A. Gardiner, Sagnac interferometry using bright matter-wave solitons, Phys. Rev. Lett. **114**, 134101 (2015).
[70] J. Polo, P. Naldesi, A. Minguzzi, and L. Amico, The quantum solitons atomtronic interference device, Quantum Sci. Technol. **7**, 015015 (2021).
[71] P. Naldesi, J. Polo, V. Dunjko, H. Perrin, M. Olshanii, L. Amico, and A. Minguzzi, Enhancing sensitivity to rotations with quantum solitonic currents, SciPost Phys. **12**, 138 (2022).
[72] I. Tutunnikov, C. Chuang, and J. Cao, Coherent spatial control of wave packet dynamics on quantum lattices, J. Phys. Chem. Lett. **14**, 11632 (2023).

[73] E. S. Sedov, A. P. Alodjants, S. M. Arakelian, Y.-L. Chuang, Y. Lin, W.-X. Yang, and R.-K. Lee, Tunneling-assisted optical information storage with lattice polariton solitons in cavity-QED arrays, Phys. Rev. A **89**, 033828 (2014).

[74] R. Cruickshank, F. Lorenzi, A. La Rooij, E. Kerr, T. Hilker, S. Kuhr, L. Salasnich, and E. Haller, Data for experimental observation of single- and multi-site matter-wave solitons in an optical accordion lattice, University of Strathclyde, 2025, 10.15129/c78af204-a552-4213-a581-7cbdaa14a311.